ACS OMEGA

Open Access

http://pubs.acs.org/journal/acsodf

Article

Insights into the Mechanism of Catalytic Activity of *Plasmodium* Parasite Malate-Quinone Oxidoreductase

Takeshi Ito,* Yuma Tojo,# Minori Fujii,# Kohei Nishino, Hidetaka Kosako, and Yasuo Shinohara

Cite This: *ACS Omega* 2024, 9, 21647−21657

Read Online

ACCESS | Metrics & More | Article Recommendations | Supporting Information

ABSTRACT: *Plasmodium* malate-quinone oxidoreductase (MQO) is a membrane flavoprotein catalyzing the oxidation of malate to oxaloacetate and the reduction of quinone to quinol. Recently, using a yeast expression system, we demonstrated that MQO, expressed in place of mitochondrial malate dehydrogenase (MDH), contributes to the TCA cycle and the electron transport chain in mitochondria, making MQO attractive as a promising drug target in *Plasmodium* malaria parasites, which lack mitochondrial MDH. However, there is little information on the structure of MQO and its catalytic mechanism, information that will be required to develop novel drugs. Here, we investigated the catalytic site of *P. falciparum* MQO (PfMQO) using our yeast expression system. We generated a model structure for PfMQO with the AI tool AlphaFold and used protein footprinting by acetylation with acetic anhydride to analyze the surface topology of the model, confirming the computational prediction to be reasonably accurate. Moreover, a putative catalytic site, which includes a possible flavin-binding site, was identified by this combination of protein footprinting and structural prediction model. This active site was analyzed by site-directed mutagenesis. By measuring enzyme activity and protein expression levels in the PfMQO mutants, we showed that several residues at the active site are essential for enzyme function. In addition, a single substitution mutation near the catalytic site resulted in enhanced sensitivity to ferulenol, an inhibitor of PfMQO that competes with malate for binding to the enzyme. This strongly supports the notion that the substrate binds to the proposed catalytic site. Then, the location of the catalytic site was demonstrated by structural comparison with a homologous enzyme. Finally, we used our results to propose a mechanism for the catalytic activity of MQO by reference to the mechanism of action of structurally or functionally homologous enzymes.

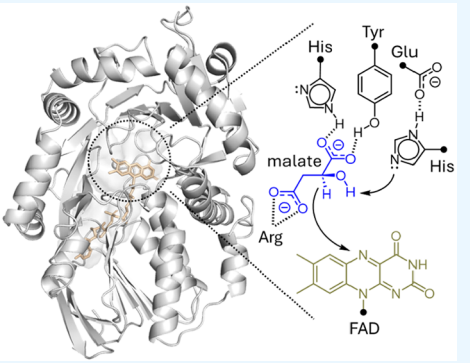

INTRODUCTION

Malate-quinone oxidoreductase (MQO), which catalyzes the oxidation of malate to oxaloacetate and the reduction of quinone to quinol, is a membrane protein containing FAD and is found in some bacteria and apicomplexan parasites.[1−4] MQO shows no homology to NAD^+-reducing malate dehydrogenase (MDH), a well-known soluble enzyme of the TCA cycle that converts malate to oxaloacetate coupled with NAD^+ reduction.[2] In *Plasmodium* parasites, which cause malaria, mitochondrial MDH is missing.[1,5−7] Thus, based on its catalytic properties, *Plasmodium* parasite MQO is thought to function in place of MDH as a TCA cycle enzyme in mitochondria, and to be coupled with the electron transport chain (ETC) through quinone reduction;[1,8−11] accordingly, *Plasmodium* MQO has received attention as a putative antimalarial target.[11−14] Recently, using a yeast expression system, we showed that *P. falciparum* MQO (PfMQO) can functionally replace yeast mitochondrial malate dehydrogenase (MDH1), clearly demonstrating that PfMQO contributes to the energy metabolism of the TCA cycle and the ETC.[15] However, as no crystal structure is yet available for MQO, we are able to say little about the mechanism of its catalytic activity, although the biochemical properties of several eukaryotic and bacterial MQOs have been studied in detail.[12,16,17]

An understanding of protein structures is critical for elucidating the functional mechanisms of proteins, for example, revealing interactions with ligand molecules, and thus allowing the development of novel drugs to regulate protein function. While the protein structures provided by X-ray crystallography, NMR spectroscopy, and cryo-EM are robust and reliable, these methods are difficult and challenging; thus, protein structures are solved more slowly than new protein sequences are determined, and the gap between the number of protein sequences available and the number of structures solved has been growing.[18] On the other hand, the recent remarkable development of computational methods to predict protein conformation from sequence has led to programs like

Received: March 18, 2024
Revised: April 19, 2024
Accepted: April 23, 2024
Published: May 1, 2024

AlphaFold and RoseTTAFold already playing a key role in the field of life sciences.[18−21] Nevertheless, although highly accurate protein structure models are now available due to such AI-based theoretical predictions, the models produced are not complete since they lack coordinates for small molecules, including ligands and cofactors, which are often required for protein function. In addition, especially flexible parts of proteins cannot be accurately characterized in the predictions.[18,21−23]

Protein footprinting, based on chemical labeling and mass spectrometry, is a strategy for probing the topography of proteins. Acetylation by acetic anhydride (Ac_2O) is a classical method of labeling the primary amine group of Lys residues, which allows protein surface structure to be probed.[24−26] As side reactions, Ac_2O can also acetylate the hydroxyl groups of Ser, Thr, and Tyr residues, the imidazole ring of His residues, and the thiol group of Cys residues.[26,27] The acetylated residues can be identified by mass spectrometry and represent chemically accessible sites on protein surfaces. This approach could be applied to investigate whether model structures predicted by the computational methods above are reliable[28] and whether cavities or tunnels in the model structures are accessible to small molecules such as ligands. Using protein footprinting together with a prediction model by AlphaFold 2.0 (AF2), this study probes a putative catalytic site in *P. falciparum* MQO and, following further biochemical analyses based on site-directed mutagenesis, we are able to propose the mechanism of catalytic activity for MQO.

RESULTS

Effect of Acetic Anhydride on MQO Activity. Protein footprinting by acetylation of Lys residues with acetic anhydride (Ac_2O), accompanied by side reactions with Ser, Thr, Tyr, His, and Cys, is the classical and most widely adopted approach used to probe protein surface structure. To probe the surface topology of MQO, we performed acetylation of PfMQO fused with a Flag-tag peptide (PfMQO-Flag), using mitochondria extracted from a yeast strain that expresses the enzyme in place of yeast mitochondrial MDH1 (Δ*Mdh1/PfMqo-Flag*), which was constructed previously.[15] First, to determine the appropriate concentrations of Ac_2O for acetylation, we checked for a concentration-dependent effect of Ac_2O on MQO activity. We expected the activity to decrease with increasing concentration of Ac_2O, but interestingly treatment with lower concentrations of Ac_2O (10−200 μM) instead enhanced enzyme activity to 1.5-fold of control at 50 and 100 μM, while higher concentrations (200−1000 μM) did indeed suppress activity to 0.4-fold that of control at 1000 μM (Figure 1). We will discuss these results below. However, for the following protein footprinting experiments, we conducted acetylation with 50 and 1000 μM Ac_2O.

Mapping of Acetylated Residues onto an AF2-Predicted Model of PfMQO. To identify the acetylated residues, and consequently some of the chemically accessible sites of PfMQO, LC-MS/MS analysis was performed. PfMQO-Flag, acetylated by either 50 or 1000 μM Ac_2O, was purified and then digested with trypsin to generate peptides for LC-MS/MS. As a control, nonacetylated PfMQO-Flag was used. Figure 2 shows the residues of PfMQO-Flag identified as acetylated sites with 0, 50, and 1000 μM Ac_2O (probability of acetylation sites is ≥99%). The number of acetylated sites increased with increasing concentration of Ac_2O, indicating

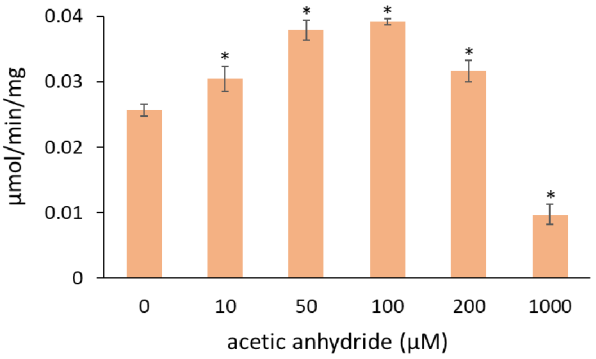

Figure 1. Concentration-dependent effect of Ac_2O on PfMQO activity in yeast mitochondria. A mitochondrial fraction was isolated from cells of the yeast strain Δ*Mdh1/PfMqo-Flag* grown in CMLE medium. Acetylation by Ac_2O was performed on this fraction. MQO activity was measured in the presence of 60 μM decylubiquinone (dUQ) and 10 mM malate as substrates, and dUQ-dependent reduction of DCIP was monitored. As a control, a mitochondrial fraction untreated with Ac_2O was used. Measurements were repeated at least three times and the error bars indicate standard deviation of the mean. Data were analyzed by Dunnett's test (*$p < 0.05$) between the control and each sample. EZR software was used.[29]

that our experiment was performed satisfactorily. The observation of acetylated sites in the control may be a result of acetylation by acetyl-CoA in cells.[30] In passing, we should note that residues that have not been identified as acetylation sites in our experiments are not necessarily chemically inaccessible.

We next mapped the acetylated residues onto a model structure predicted by AF2 (Figure 3A). The AF2-prediction model was generated from the sequence of PfMQO, in which for simplification its putative mitochondrial targeting peptide (M1-I66), which was predicted by MitoFates[32] and is not present in similar sequences of bacterial MQO, was excluded (Figure S1). With the exception of two residues (K167, S240), the acetylated sites identified by protein footprinting were located on the surface of the model structure, suggesting that the prediction is reasonably accurate. In addition, the model formed a large tunnel, which is likely to accommodate FAD (Figure 3B,C). Importantly, the acetylation analysis suggests that chemicals are able to access to the tunnel to a certain depth since some internal residues, i.e., S113, H343, and at least one of S119, T121, or H123, were assigned as acetylatable sites after treatment with 50 and/or 1000 μM Ac_2O (Figures 2 and 3C). It should be noted that there is no Lys residue, a main target of acetylation, within the tunnel, but acetylation did take place as evidenced by the side reactions. Both acetylatable His residues (H123, H343; putative and determined, respectively) are located in a shallow area near the tunnel entrance. They are sterically adjacent to E128 and D345 in the model, respectively, raising the possibility that either H123 or H343 (or both) might participate in a His-Glu/Asp pair, which is typically required for a proton relay system in the catalytic sites of 2-hydroxyacid dehydrogenases, including MDH (Figure 3C). His-Asp (or -Glu) interactions in such catalytic sites serve to keep the imidazole ring of His in the desired orientation, allowing the free imidazole-*N* to act as both proton acceptor and donor.[33] In addition, there are two Tyr residues (Y236, Y330) in the vicinity (Figure 3C). In oxidoreductases, it is commonly found that His plays a role in proton transfer and Tyr is also capable of this role.[34] Thus, we

https://doi.org/10.1021/acsomega.4c02614
ACS Omega 2024, 9, 21647−21657

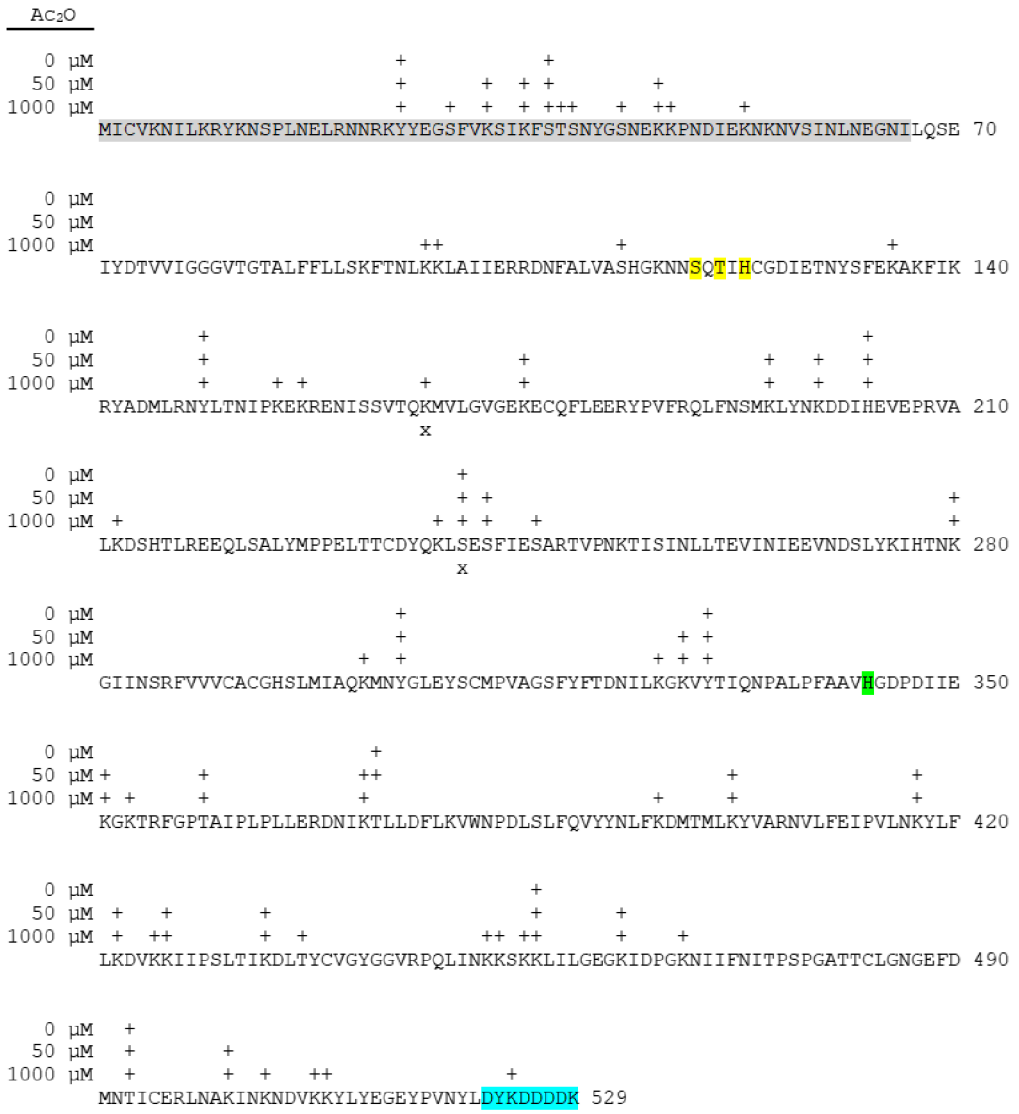

Figure 2. Acetylation residues as chemically accessible sites in PfMQO. A mitochondrial fraction was isolated from yeast cells of Δ*Mdh1*/*PfMqo*-*Flag* grown in CMLE medium. Acetylation by 50 or 1000 μM Ac_2O was performed using this fraction. As a control, a nonacetylated mitochondrial fraction was prepared. PfMQO-Flag was purified by anti-Flag immunoprecipitation and digested with trypsin. The tryptic peptides were analyzed by LC-MS/MS. Probability of acetylation at each site was determined by ptmRS.[31] Plus signs (+) indicate identified acetylation sites (threshold of probability of acetylation: 99%). X signs indicate acetylation at nonsurface residues in a PfMQO model predicted by AlphaFold2. The probability of acetylation especially at residues inside the tunnel observed in the model was individually checked. The probability at S119, T121, and H123 in a single-acetylated peptide was 32.83−33.23%, which means that one of the three residues is likely to be the true acetylation site (shown in yellow), and that at H343 was 98.62% (shown in green). Gray and blue represent the putative mitochondrial targeting peptide and the Flag-tag, respectively.

decided to perform mutagenesis studies to characterize these His and Tyr residues further.

Contribution of H123, H343, Y236, and Y330 to Catalytic Function. To verify the importance of the H123, H343, Y236, and Y330 residues for the catalytic function of PfMQO, we constructed the following strains by site-directed mutagenesis: Δ*Mdh1*/*PfMqo*-H123A-*Flag*, Δ*Mdh1*/*PfMqo*-H343A-*Flag*, Δ*Mdh1*/*PfMqo*-Y236F-*Flag*, and Δ*Mdh1*/*PfMqo*-Y330F-*Flag*. The plasmids encoding each PfMQO-Flag mutant were prepared by overlap extension PCR[35] and introduced into the Δ*Mdh1* yeast strain (see Materials and Methods). As we reported previously, the Δ*Mdh1* strain, lacking mitochondrial malate dehydrogenase, shows a growth defect on acetate (nonfermentable carbon source), but can grow on glucose (fermentable carbon source), and the growth defect on acetate is complemented by expressing PfMQO-Flag.[15] Therefore, the functionality of the mutated enzymes was first evaluated by a simple growth test (Figure 4). With the exception of the Y236F mutant, the strains were unable to grow on acetate plates, similarly to the Δ*Mdh1* strain, while all strains grew well on glucose plates. The results suggest that H123, H343, and Y330, but not Y236, are functionally essential, which is consistent with the fact that these three residues are conserved in both bacterial and apicomplexan MQOs, while Y236 is replaced by Phe in some organisms (Figure S1).

To gain some insight into the severity of the effect of the mutations, we compared the enzyme activity of WT PfMQO with that of the mutants using mitochondria from the various yeast strains. Consistent with the growth tests, the single substitutions at H123, H343, and Y330 caused a drastic loss of enzyme activity (Figure 5), suggesting that these residues are

https://doi.org/10.1021/acsomega.4c02614
ACS Omega 2024, 9, 21647−21657

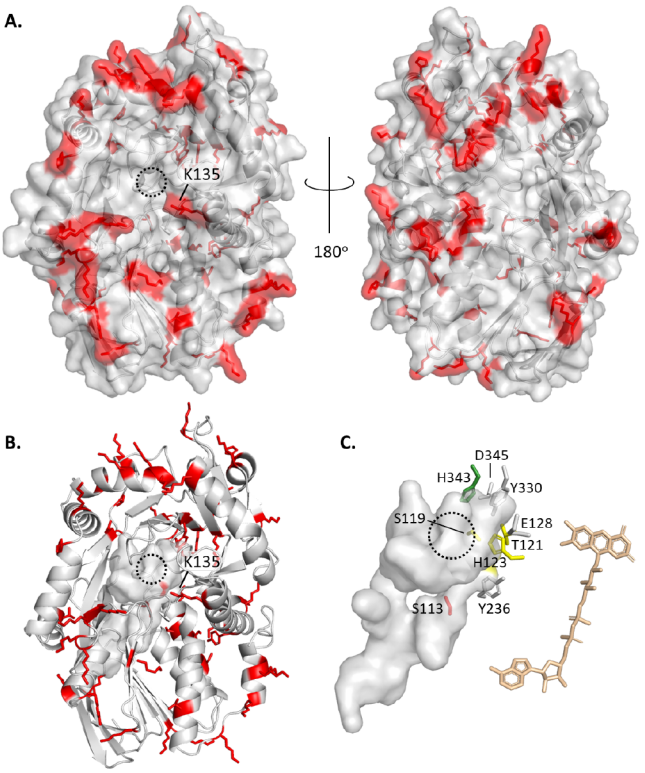

Figure 3. PfMQO model structure predicted by AlphaFold2. Using AlphaFold2, a model structure of PfMQO was generated from the protein sequence, excluding a putative mitochondrial targeting peptide (M1-I66). (A) The acetylation sites identified experimentally are mapped onto the model and are shown in red with their side chains shown as sticks. (B) A tunnel formed in the model is represented with the tunnel entrance shown as dotted circles here and in C. Acetylatable K135 is located outside the tunnel entrance. (C) Identified or possible acetylation sites (S113, S119, T121, H123, H343) in the tunnel are shown, and the tunnel volume is compared with the molecular size of FAD. H123 and E128, or H343 and D345 seem to form a His-Glu or His-Asp pair, respectively, by analogy with MDH.[33] The Tyr residues (Y236 and Y330) subjected to mutagenesis (see below) are also represented. The membrane-binding site(s) of PfMQO remain unidentified, although the acetylated sites that are chemically accessible are unlikely to interact closely with the membrane.

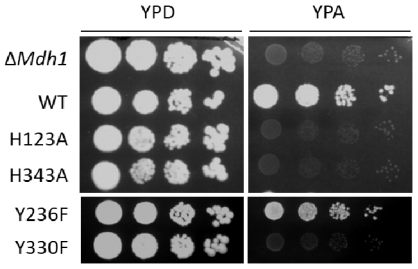

Figure 4. Growth phenotypes of yeast strains on fermentable and nonfermentable plates. Δ*Mdh1* and Δ*Mdh1* expressing WT or mutant forms of PfMQO-Flag, grown in SD medium, were serially diluted and spotted onto agar plates. The plates were incubated at 30 °C for 3 days. YPD contains 2% glucose (fermentable carbon source). YPA contains 2% acetate (nonfermentable carbon source).

important for catalysis. The result is similar to that of Δ*Mdh1* under the experimental conditions used.[15]

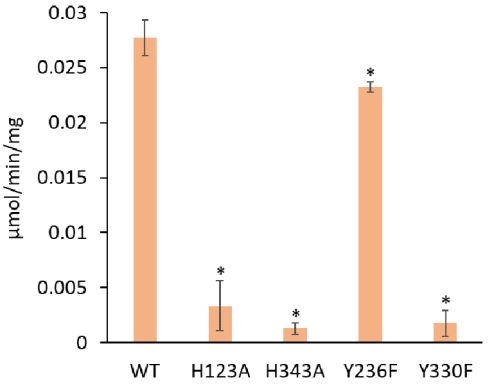

Figure 5. Measurements of PfMQO activity in yeast mitochondria. A mitochondrial fraction was isolated from yeast strains (Δ*Mdh1* expressing PfMQO-Flag WT or mutants) grown in CMLE medium. The MQO activity was measured in the presence of 60 μM decylubiquinone (dUQ) and 10 mM malate as substrates, and dUQ-dependent reduction of DCIP was monitored. Measurements were repeated at least three times and the error bars indicate standard deviation of the mean. Data were analyzed by Dunnett's test (*$p < 0.05$) between WT and each mutant. EZR software was used.[29]

While some mutations might also somewhat affect protein stability, the consistency with the growth test results rules out the possibility that the loss of activity would be entirely due to protein denaturation during the isolation of mitochondria and enzyme activity assay. In addition, under conditions with 10-fold higher concentrations of the substrates (600 μM decylubiquinone, 100 mM malate), we found essentially no significant difference in MQO activity of the mutants compared with the results of Figure 5, i.e., their activity was similar to that of the Δ*Mdh1* strain alone. This suggests that the loss of activity in the mutants was due to a loss of functional ability rather than decreased affinity for the substrates (Figure S2). We should note that, under the assay conditions used in Figure S2, the Δ*Mdh1* and mutant strains had moderate substrate-dependent DCIP-reducing activities, possibly due to malate oxidation by mitochondrial succinate dehydrogenase.[15,36,37] However, this nonspecific activity is nondetectable under conditions with 60 μM decylubiquinone and 10 mM malate.[15] Finally, to rule out the possibility that our observations might reflect changes in protein expression levels, we analyzed mitochondria extracted from each strain by Western blotting using an anti-Flag antibody. WT and mutant extracts showed a clear band around 60 kDa corresponding to PfMQO-Flag; the signals were of similar strength, although that from the H123A mutant was slightly weaker, confirming that the loss of activity in the H343A and Y330F strains, at least, is due to a functional defect (Figure 6). Densitometry of the bands, performed using ImageJ software,[38,39] showed that the intensity of the band representing the H123A mutant was about 2.7-fold less than that in WT, which was reproduced in repeated experiments. While this is a marked difference, it is unlikely to explain the drastic loss of enzyme activity observed, which means that the H123 residue is also essential for catalytic function, although this mutation might also affect the expression level of the variant protein in mitochondria. In summary, mutagenesis study showed that H123, H343, and the adjacent Y330 are essential for the function of PfMQO. Thus, again, the protein footprinting results combined with the AF2 prediction model strongly suggest that the chemically

https://doi.org/10.1021/acsomega.4c02614
ACS Omega 2024, 9, 21647−21657

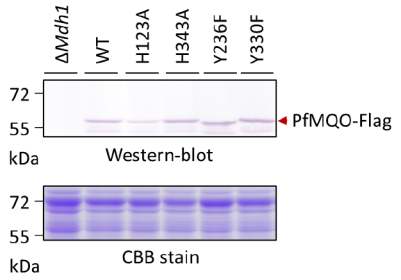

Figure 6. Western-blot analysis of the expression of PfMQO in yeast mitochondria. A mitochondrial fraction was isolated from yeast strains (Δ*Mdh1* and Δ*Mdh1* expressing PfMQO-Flag WT or mutants) grown in CMLE medium. The fractions (10 μg protein) were subjected to 10% Laemmli SDS-PAGE and Western blotting. For detection, an antibody against the Flag-tag at the C-terminus of PfMQO was used. CBB: Coomassie brilliant blue.

accessible shallow area of PfMQO near the tunnel entrance is a catalytic site.

Characterization of Inhibitor- and Substrate-Binding Site. Substitution of Lys by Gln or Asn can mimic *N*-acetylated Lys,[40] potentially leading to activity enhancement, we explored the effect of such a substitution for a number of Lys residues in PfMQO, since this might improve our understanding of the catalytic mechanism. Although we found no enhancement of enzyme activity by substitution of these residues (data not shown), the substitution of K135Q provided an important insight into the location of the malate-binding site. The mutation at acetylatable K135, located outside the tunnel entrance (Figure 3A,3B), significantly enhanced sensitivity to ferulenol (Figure 7B). Ferulenol is a

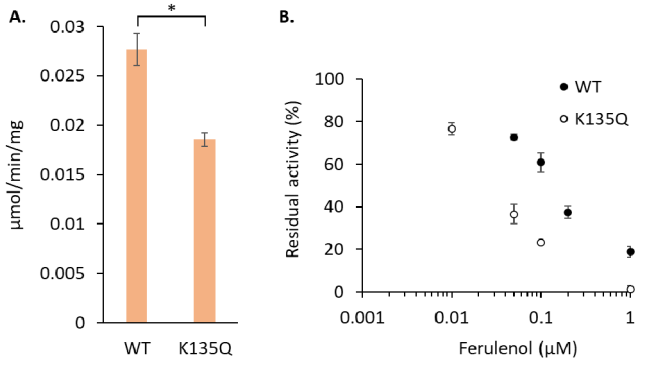

Figure 7. PfMQO activity and inhibitor sensitivity of K135Q mutant. A mitochondrial fraction was isolated from yeast strains (Δ*Mdh1* expressing PfMQO-Flag WT or K135Q) grown in CMLE medium. (A) The MQO activity was measured in the presence of 60 μM decylubiquinone (dUQ) and 10 mM malate as substrates, and dUQ-dependent reduction of DCIP was monitored. (B) Residual activity in the presence of an MQO inhibitor, ferulenol. Measurements were repeated at least three times and the error bars indicate standard deviation of the mean. Data were analyzed by an unpaired *t* test (*$p < 0.05$) between WT and K135Q.

potent inhibitor of MQO and is competitive with malate rather than quinone, in spite of its quinone-like structure.[12] We confirmed that the activity of the mutated enzyme (K135Q) was moderately similar to that of WT (Figure 7A), which was consistent with a growth test (Figure S3).

In addition, the PfMQO expression level in the mitochondria of this strain was similar to that of WT (Figure 8). This

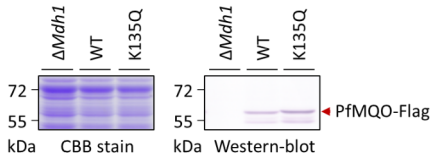

Figure 8. Western-blot analysis of the expression of PfMQO-K135Q in yeast mitochondria. A mitochondrial fraction was isolated from yeast strains (Δ*Mdh1* and Δ*Mdh1* expressing PfMQO-Flag WT or K135Q) grown in CMLE medium. The fractions (10 μg protein) were subjected to 10% Laemmli SDS-PAGE and Western blotting. For detection, an antibody against the Flag-tag at the C-terminus of PfMQO was used. CBB: Coomassie brilliant blue.

indicates that the chemically accessible K135 residue is adjacent to the malate-binding site overlapping with the inhibitor-binding site. This observation is in accordance with the location of the catalytic site of PfMQO as determined by the protein footprinting and mutagenesis results above, combined with the AF2 prediction model.

DISCUSSION

In this study, we characterized the surface protein topology of PfMQO by acetylation with Ac_2O using a PfMQO-Flag-expressing yeast strain, and obtained results consistent with an AF2 model of PfMQO. In addition, we found that the model predicts the presence of a large tunnel in PfMQO, likely to accommodate the cofactor FAD, which is chemically accessible to a certain depth. The putatively acetylatable H123 and acetylatable H343 residues are adjacent to E128 or D345, respectively, in a shallow area near the tunnel entrance, likely each corresponding to a His-Glu/Asp pair. Such amino acid pairs form part of a proton relay system that is typical of the catalytic sites of 2-hydroxyacid dehydrogenases (e.g., MDH).[33] Mutagenesis studies, together with growth tests, enzyme activity measurements, and Western-blot analysis, demonstrated that H123, H343, and the adjacent Y330 are essential for the function of PfMQO. Moreover, a substitution of K135, which is located outside the tunnel entrance, resulted in a significant change in sensitivity to ferulenol, a competitive inhibitor that interferes with malate binding. Altogether, these observations indicate that FAD is accommodated in the tunnel and, in particular, its flavin site, which needs to be accessible to the substrates, is located in the shallow area near the tunnel entrance.

To explore whether the tunnel of the prediction model can accommodate FAD, the model was overlaid on a crystal structure of FAD-dependent glycerophosphate oxidase from *Mycoplasma pneumoniae*(MpGlpO; PDB 4X9M). MpGlpO is quite similar to PfMQO (NCBI Standard Protein BLAST showed 56% coverage, 23% identity). As shown in Figure 9A, the two enzymes superimpose well (RMSD 5.3 Å), and the tunnel in PfMQO seems to bind FAD in a manner like that observed in MpGlpO.[41] This is supported by the number of residues surrounding FAD that are well conserved and similarly placed in MpGlpO and MQO (Figures 9B and S1 and S4). In addition, more recently, a crystal structure of another FAD-dependent enzyme, mitochondrial L-2-hydroxyglutarate dehydrogenase from *Drosophila melanogaster* (DmL2HGDH; PDB 8W78), was reported.[42] DmL2HGDH is much more similar to PfMQO (NCBI Standard Protein BLAST showed 74% coverage, 22% identity) and superimposes very closely on it (RMSD 2.3 Å; Figure 9A). This

https://doi.org/10.1021/acsomega.4c02614
ACS Omega 2024, 9, 21647−21657

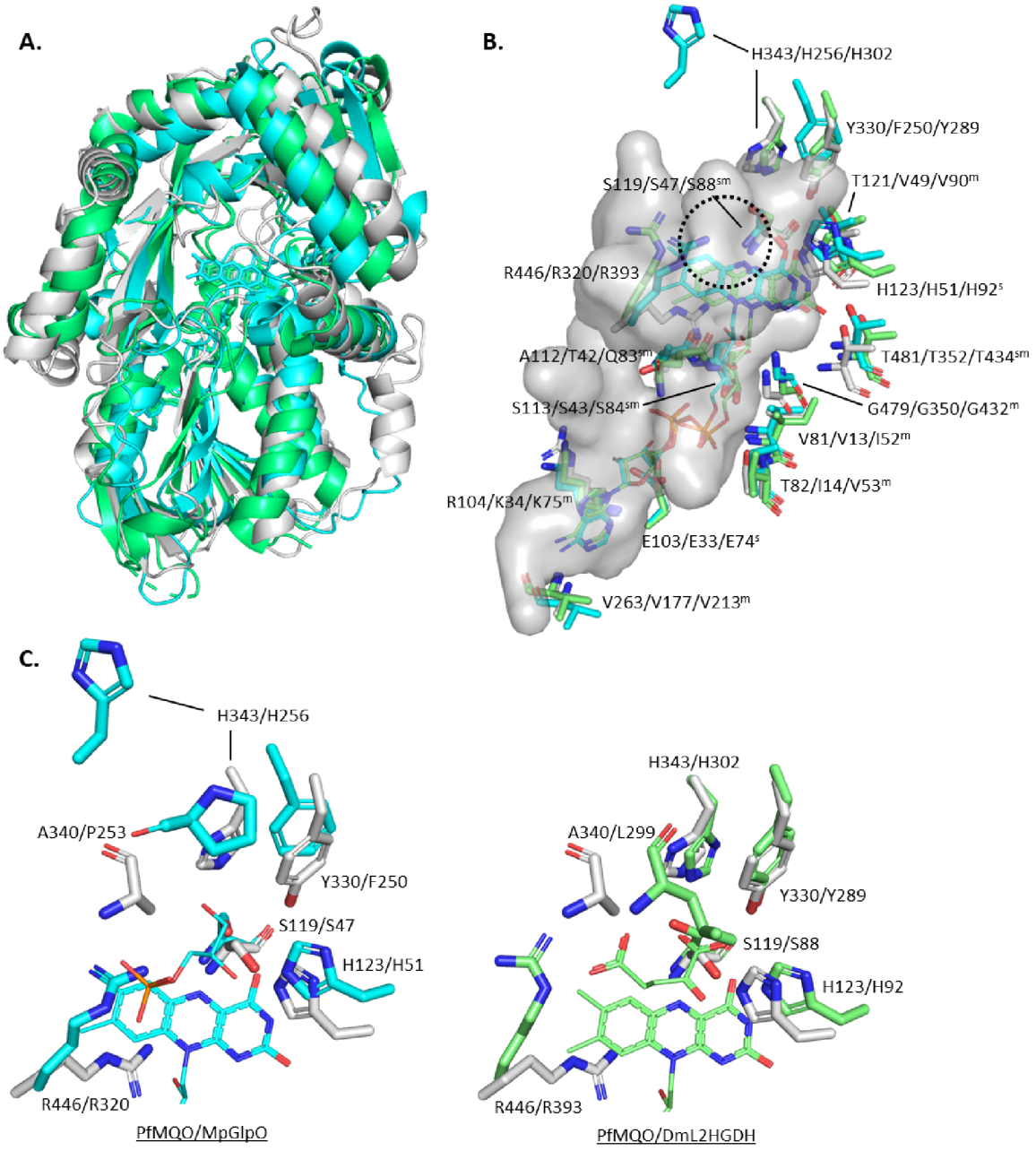

Figure 9. Superimposition of PfMQO, FAD-dependent *Mycoplasma* glycerophosphate oxidase and *Drosophila* L-2-hydroxyglutarate dehydrogenase. (A) The model structure of PfMQO (gray) and FAD-bound crystal structures of FAD-dependent glycerophosphate oxidase from *Mycoplasma pneumoniae* (MpGlpO; PDB 4X9M; cyan) and L-2-hydroxyglutarate dehydrogenase from *Drosophila melanogaster* (DmL2HGDH; PDB 8W78; light green) were overlaid using PyMOL software (PyMOL molecular graphics system, version 2.6.0a0 Schrödinger, LLC; RMSD 5.3 and 2.3 Å, respectively). NCBI Standard Protein BLAST showed that the coverage and identity of MpGlpO and DmL2HGDH in amino acid sequences, compared with PfMQO, are 56% and 23%, and 74% and 22%, respectively. (B) The tunnel of the model and the FAD molecules bound to MpGlpO or DmL2HGDH are represented. The residues (PfMQO/MpGlpO/DmL2HGDH) surrounding FAD, particularly those forming hydrogen bonds with FAD in DmL2HGDH, are represented, with "s" and "m" indicating the formation of hydrogen bonds between FAD and residue side chains or main chains, respectively.[42] Also, some key residues that interact with the substrate in DmL2HGDH are shown (DmL2HGDH-S88, H92, -Y289, -H302, and -R393).[42] The entrance to the tunnel in the model is shown as a dotted circle. (C) Glycerophosphate (substrate) and 2-oxoglutarate (product) bound to MpGlpO and DmL2HGDH, respectively. The residues (PfMQO/MpGlpO, PfMQO/DmL2HGDH) around the ligand-binding sites are represented. While some residues that use the main chains (and side chains) for FAD-binding are not well conserved, almost all the key residues are located similarly in the three proteins, except for MpGlpO-H256. PfMQO-H343 does not overlay with MpGlpO-H256, but with DmL2HGDH-H302, and the position of MpGlpO-H256 makes it unlikely that it participates in catalysis.[41] The membrane-binding site(s) of PfMQO remain unidentified.

superimposition also indicated that PfMQO accommodates FAD in a manner similar to that described for DmL2HGDH by Yang et al. (Figures 9B and S4).[42] While several residues of DmL2HGDH, which interact with FAD via hydrogen bonds, are not conserved in MQO (or MpGlpO), these points of interaction are formed by the main chains (and side chains) of the residues rather than solely by their side chains (Figures 9B and S1).[42]

https://doi.org/10.1021/acsomega.4c02614
ACS Omega 2024, 9, 21647−21657

Moreover, the functionally essential H123, H343, and Y330 residues are placed around the flavin site to which the substrates need access (Figure 9B). This is consistent with their chemical accessibility as determined by protein footprinting and does not conflict with the location of the malate-binding site indicated by the analysis of the K135 substitution mutation. Thus, we conclude that FAD is accommodated in the tunnel, and its flavin site is located in the shallow area near the tunnel entrance. Interestingly, residues that interact with substrates in MpGlpO or DmL2HGDH are partially or well conserved in MQO, respectively (Figures 9B,C and S1).[41,42] Particularly in DmL2HGDH, the corresponding residues of H123, H343, and Y330 are functionally essential,[42] which is consistent with our results.

H123 corresponds to MpGlpO-H51 and DmL2HGDH-H92, which have been proposed to deprotonate the *C*2-hydroxyl of their substrate (glycerophosphate or 2-hydroxyglutarate, respectively) and form a corresponding ketone after hydride transfer from *C*2 to flavin-*N*5.[41,42] Similar to MpGlpO-H51 and DmL2HGDH-H92, a His residue in MDH that forms part of a His-Asp pair accepts the *C*2-hydroxyl proton of malate to produce oxaloacetate after hydride extraction from *C*2.[33,43] Furthermore, H343 and Y330 correspond to DmL2HGDH-H302 and -Y289, respectively, in which the imidazole ring and phenol hydroxyl group have been shown to interact with the *C*1-carboxyl of 2-hydroxyglutarate via hydrogen bonds.[42] It is interesting to note that the corresponding residues of MpGlpO (MpGlpO-H256 and -F250, respectively) seem not to participate in this role (Figure 9B,C), possibly reflecting the lack of a carboxyl at *C*1 in its substrate (glycerophosphate; hydroxyl at *C*1). The different placement of MpGlpO-H256 and PfMQO-H343 may be because MpGlpO lacks residues corresponding to PfMQO-Q333-F339 (Figure S1). On the other hand, the phosphate group of glycerophosphate interacts with MpGlpO-R320.[41] In DmL2HGDH, R393 interacts with the other carboxyl of its substrate; this residue is important but not essential for activity.[42] Similarly, the side chain of the corresponding residue in PfMQO (R446) probably interacts with the *C*4-carboxyl of malate, although its orientation needs to be refined in the model (Figure 9B,C). In summary, we propose that the oxidation of malate by PfMQO is conducted through proton/hydride transfer mediated by H123 in the shallow area near the tunnel entrance. During catalysis, both H343 and Y330 are required for correct binding of malate rather than as proton/hydride mediators. Our proposed mechanism of catalytic activity in MQO is summarized in Figure 10.

As proposed in Figure 10, the His-Glu pair of PfMQO (H123-E128), which is widely conserved among other examples of MQO (Figure S1), acts as a proton acceptor for the *C*2-hydroxyl of malate, allowing the formation of oxaloacetate after hydride extraction from *C*2 to *N*5 of flavin, as occurs in various structurally or functionally homologous enzymes. It is interesting to note that a His-mediated reaction mechanism has been proposed in *Staphylococcus* MQO, classified into a different subgroup from PfMQO,[44] after comparison with a crystal structure of the homologous enzyme, *Streptococcus* GlpO[45] which shows no similarity to PfMQO at least in amino acid sequence (NCBI Standard Protein BLAST). On the other hand, H343 and Y330 are required for correct binding of malate, which is consistent with the fact that the closely placed His residues (H123 and H343) are both required for activity, which means that these His residues have

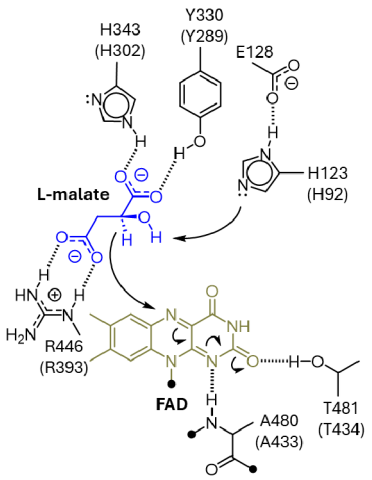

Figure 10. Schematic drawing showing the proposed mechanism of catalytic activity in MQO. The numbering of the residues corresponds to PfMQO. Some residues in DmL2HGDH, corresponding to those of PfMQO, are also represented in brackets for reference. Similar to the catalysis of DmL2HGDH, MpGlpO, and MDH,[33,41−43] the *C*2-hydroxyl of malate is extracted by the His residue of the H123-E128 pair. In addition, the *C*1- and *C*4-carboxyls of malate interact with H343 and Y330, and R446, respectively, like the interactions between DmL2HGDH and 2-hydroxyglutarate. The interaction of R446 has been similarly characterized in the corresponding residue of MpGlpO, i.e., R320. Oxaloacetate is produced by forming a ketone after hydride transfer from *C*2 to flavin-*N*5. The resulting negative charge at flavin-*N*1 and -*O*2′ in the reduced FAD is stabilized by A480 and T481, respectively, as described for MpGlpO-L351 and -T352.

distinct roles that cannot compensate for each other. Furthermore, the substitution of Y330F shows that the phenol hydroxyl group of this tyrosine is essential for enzyme function. Although the residue was detected in both nonacetylated and acetylated forms in the absence of Ac_2O (Figure 2), and thus a proportion of the residue could be acetylated by acetyl-CoA in cells, nonacetylated Y330, rather than the acetylated from, is likely to represent the functional form according to the crystal structure of DmL2HGDH bound to 2-oxoglutarate.[42]

Our present study provides important and fundamental insights into both the mechanism of catalytic activity of MQO and the nature of the inhibitor-binding site, which should be invaluable for the design of novel drugs that target MQO. On the other hand, we should note that the catalysis of PfMQO follows a sequential, ordered bibi mechanism[12] and thus the active site must accommodate both malate and quinone concurrently; however, the AF2-predicted structure seems not to allow enough space for this (Figure 9B), which means that the model may not reflect a conformation where both substrates are bound. Also, to date, we have no definite insight into the mode of quinone reduction in PfMQO. In general, there are a variety of potent inhibitors, all of which bind to the quinone reaction site in a variety of oxidoreductases that use quinones as substrates.[46−48] This implies that the quinone-binding site is a possible druggable site in MQO. Using several approaches including drug screening, compounds have been identified that might inhibit MQO.[12,14,49,50] However, to the best of our knowledge, no inhibitor has been yet reported that interacts with the quinone-binding site. To explore novel inhibitors targeting MQO, it will be necessary to fully understand the mechanism of action of MQO, for example, by solving the structure of enzyme−substrate complexes.

https://doi.org/10.1021/acsomega.4c02614
ACS Omega 2024, 9, 21647−21657

Molecular docking followed by molecular dynamics simulations would also provide important hints about the quinone site and would allow the binding of ferulenol to be characterized in more detail. This will be included in our future work on the design of potent inhibitors specific to MQO. The activity enhancement observed in acetylated MQO also provides important clues as to catalytic mechanism. We note that the activity enhancement was only 1.5-fold, but this is likely the net result of both enhancement and suppression, which means that the activity could be enhanced more strongly in vivo if MQO could be acetylated site-selectively. It is known that some TCA cycle enzymes can be either activated or deactivated by acetylation, where the source of the acetyl groups is thought to be acetyl-CoA. The functional homologues of MQO, malate dehydrogenases (MDH), including a cytoplasmic isoform, are examples where acetylation results in activation.[30,51−53] Indeed, our results indicate that the activity of MQO may depend on the concentration of acetyl-CoA in vivo. Therefore, we are planning to identify residues that contribute to this effect, which could provide further important insights into the catalytic mechanism and regulation of function of MQO.

CONCLUSIONS

Our results, based on protein footprinting and mutagenesis study combined with structural modeling using AlphaFold, reveal the catalytic site of PfMQO. Our findings are strongly supported by structural comparison with the homologous enzymes, MpGlpO and DmL2HGDH. Moreover, using our results, we propose a catalytic mechanism of PfMQO by reference to the catalysis of such structurally or functionally homologous enzymes. These insights into the mechanism of catalytic activity of MQO should be invaluable for the design of novel drugs that target MQO.

MATERIALS AND METHODS

Strains and Growth Conditions. Strains of *Saccharomyces cerevisiae* were grown as described previously.[15] Briefly, cells were grown at 30 °C on synthetic minimal medium (0.67% yeast nitrogen base without amino acids; BD Difco) supplemented with 2% glucose, essential amino acids, and other nutrients to meet auxotrophic requirements (SD). The strains were also grown on YP medium (1% yeast extract, Nacalai Tesque; 2% hipolypepton N, Fujifilm Wako Pure Chemical Corporation) with 2% glucose (YPD) or 2% potassium acetate (YPA), or in complete medium (1% yeast extract, 0.1% potassium phosphate, 0.12% ammonium sulfate, pH 5.5) with 2% sodium lactate with pH 5.5 and 2% ethanol (CMLE). Solid media contained 2% agar. When needed, 0.2 mg/mL geneticin (G418 sulfate) was added. *E. coli* strains were grown at 37 °C in LB medium. When needed, 80 μg/mL ampicillin was added.

Site-Directed Mutagenesis, Construction of Plasmids, and Yeast Transformation. A series of plasmids harboring the *PfMqo-Flag* gene, encoding C-terminally Flag-tagged PfMQO (Uniprot C6KT09), with nucleotide substitutions was constructed by site-directed mutagenesis based on overlap extension PCR.[35] *PfMqo-Flag* previously cloned into a centromere vector, containing a promoter of the yeast mitochondrial ADP/ATP carrier 2 gene, was used as template (pRS314-YA2P/*PfMqo-Flag*).[15,54] Left-half and right-half fragment pairs were amplified and assembled into full-length genes using the primers listed in Table S1. The PCR product was then digested with *Nde*I and *Bam*HI and inserted into the pRS314-YA2P vector to construct plasmids expressing PfMQO-Flag with each of the following single mutations: H123A, K135Q, Y236F, Y330F, or H343A. Then, a Δ*Mdh1* yeast strain, lacking mitochondrial malate dehydrogenase, was transformed by the lithium acetate method[55] with the constructed plasmids. For the selection of transformants, SD agar plates lacking tryptophan, in the presence of 0.2 mg/mL G418 sulfate, were used.

Extraction of Yeast Mitochondria. A mitochondrial fraction was isolated from yeast cells grown in CMLE as described previously.[15] Cells were harvested by centrifugation (3000 × *g*, 4 min), washed with water, and resuspended in 0.1 M Tris-H_2SO_4 pH 8, 10 mM dithiothreitol (2 mL per g wet cell weight). After incubating the suspension for 15 min at 30 °C with shaking at 70 rpm, cell pellets were collected by centrifugation (3000 × *g*, 4 min) and washed with buffer 1: 20 mM KPi pH 7.4, 1.2 M D-sorbitol. Then, cell pellets were resuspended in buffer 1 (6.7 mL per g wet cell weight) containing zymolyase-T20 (10 mg per g wet cell weight; Nacalai Tesque). After incubating the suspension for 45 min at 30 °C with shaking at 70 rpm, the resulting spheroplasts were collected by centrifugation (2200 × *g*, 7 min, 4 °C), washed with buffer 1, and resuspended in buffer 2: 10 mM Tris-HCl pH 7.4, 0.6 M D-mannitol, 2 mM EDTA, 1 mg/mL fatty acid-free BSA (6.7 mL per g wet cell weight). The suspended spheroplasts were then lysed using a Dounce homogenizer (ten strokes of a tight-fitting pestle), after which homogenates were centrifuged (2000 × *g*, 10 min, 4 °C) to remove unbroken cells and debris. After an additional centrifugation (7800 × *g*, 10 min, 4 °C) of the supernatant, a mitochondrial fraction (pellet) was obtained. The mitochondrial fraction was resuspended in buffer 2 (50 μL per g wet cell weight) and stored at −80 °C until use.

Acetylation of Mitochondrial Fraction. A mitochondrial fraction was isolated from the Δ*Mdh1*/*PfMqo-Flag* strain grown in CMLE and was resuspended (0.2 mg/mL) in ice-cold reaction buffer (500 μL) containing 50 mM HEPES-KOH pH 7, 0.65 M D-sorbitol and placed on ice for 2 min. Acetylation was initiated by adding an appropriate concentration of Ac_2O solved in acetonitrile (1 μL). For a control experiment, acetonitrile (1 μL) alone was added. After incubating for 20 min on ice, 10 mM imidazole was added to the mixture. Then, the acetylated mitochondrial fraction (pellet) was collected by centrifugation (16 100 × *g*, 10 min, 4 °C). For LC-MS/MS analysis, the acetylated mitochondrial pellets were stored at −80 °C until use. For activity measurements, the pellets were resuspended in ice-cold assay buffer (30 μL) containing 50 mM HEPES-KOH pH 7 and kept on ice until use.

Malate-Quinone Oxidoreductase Activity. Malate-dependent ubiquinone reduction in the mitochondrial fractions was measured spectrophotometrically at 37 °C in a quartz cuvette as described previously,[15] with some modifications when necessary. DCIP, which is reduced by the ubiquinol produced, was used as an indicator. The DCIP reduction was monitored by plotting the absorbance change at 600 nm (ε = 21 mM^{-1} cm^{-1}). Mitochondrial fractions (0.05 mg/mL) and 120 μM DCIP (Sigma-Aldrich) were added to the assay buffer (1.8 mL) with 2 μM antimycin A. After incubating for 1 min, 60 μM decylubiquinone (dUQ; Enzo Life Sciences) was added. Following an additional incubation

https://doi.org/10.1021/acsomega.4c02614
ACS Omega 2024, 9, 21647−21657

for 1 min, the reaction was initiated by adding 10 mM L-malate. For the evaluation of inhibitor sensitivity, an appropriate concentration of ferulenol (Adipogen Life Sciences) was added to the assay buffer. Where indicated, 600 μM dUQ and 100 mM L-malate were added. For a given condition, activity values were calculated by subtracting a DCIP-independent nonspecific absorbance change, which was observed when 600 μM dUQ and 100 mM malate were used. For activity measurements in the acetylated mitochondria, the mitochondrial suspension (30 μL) was diluted to 0.1 mg/mL with assay buffer (970 μL) at 37 °C. The suspension (900 μL) was then added to the assay buffer (900 μL) in a quartz cuvette. After adding 2 μM antimycin A, the above procedure was continued. Mitochondria used in the present study were not fully intact, as they had been frozen once. Thus, membrane-impermeable malate is accessible to the catalytic site located in the mitochondrial matrix, while some may access the site via outer mitochondrial membrane-bound voltage-dependent anion channels and the inner mitochondrial membrane-bound dicarboxylate carrier.[15] dUQ and DCIP are membrane-permeable. Activity measurements were repeated at least three times.

Purification of PfMQO-Flag and LC-MS/MS Analysis. The acetylated mitochondrial pellets were lysed in RIPA buffer (500 μL) containing 20 mM HEPES-NaOH pH 7.5, 1 mM EGTA, 1 mM $MgCl_2$, 150 mM NaCl, 0.25% sodium deoxycholate, 0.05% SDS, 1% NP-40, complete protease inhibitor cocktail, and 50 units/mL benzonase. After centrifugation (20 000 × *g*, 15 min, 4 °C), the supernatants were incubated for 2 h at 4 °C with anti-FLAG M2 magnetic beads (Sigma-Aldrich). The beads were washed three times with RIPA buffer and then twice with 50 mM ammonium bicarbonate. Proteins on the beads were digested by adding 200 ng trypsin/Lys-C mix (Promega) for 16 h at 37 °C. The digests were reduced, alkylated, acidified, and desalted with GL-Tip SDB tip columns (GL Sciences). The eluates were evaporated and dissolved in 0.1 trifluoroacetic acid and 3% acetonitrile (ACN). LC-MS/MS analysis of the resultant peptides was performed on an EASY-nLC 1200 UHPLC instrument connected to an Orbitrap Fusion mass spectrometer through a nanoelectrospray ion source (Thermo Fisher Scientific). The peptides were separated on a 75 μm inner diameter × 150 mm C18 reversed-phase column (Nikkyo Technos) with a linear 4−32% ACN gradient for 0−100 min followed by an increase to 80% ACN for 10 min and a final hold at 80% ACN for 10 min. The mass spectrometer was operated in data-dependent acquisition mode with a maximum duty cycle of 3 s. MS1 spectra were measured with a resolution of 60 000, an automatic gain control (AGC) target of 4e5, and a mass range of 350−1500 m/z. HCD MS/MS spectra were acquired in the Orbitrap with a resolution of 30 000, an AGC target of 5e4, an isolation window of 1.6 m/z, a maximum injection time of 54 ms, and a stepped collision energy of 25, 30, and 35. Dynamic exclusion was set to 15 s. Raw data were directly analyzed against the SwissProt database restricted to *S. cerevisiae* supplemented with the PfMQO-Flag sequence using Proteome Discoverer 2.5 (Thermo Fisher Scientific) with the Sequest HT search engine. The search parameters were as follows: (a) trypsin as an enzyme with up to two missed cleavages; (b) precursor mass tolerance of 10 ppm; (c) fragment mass tolerance of 0.02 Da; and (d) carbamidomethylation of cysteine, oxidation of methionine, and acetylation of protein N-terminus, cysteine, histidine, lysine, serine, threonine, and tyrosine as variable modifications. Peptides were filtered at a false discovery rate of 1% using the Percolator node.

Prediction of PfMQO Model Structure by AlphaFold. A model structure of PfMQO was generated by the notebook "ColabFold v1.5.3: AlphaFold2 using MMseqs2"[56,57] with default settings on 21 December 2023. The input protein sequence was PfMQO (Uniprot C6KT09) lacking a putative mitochondrial targeting peptide (**M1-I66**, Figure S1). To compare the model with MpGlpO and DmL2HGDH (PDB 4X9M and 8W78, respectively), the structures were overlaid and aligned using PyMOL software (PyMOL molecular graphics system, version 2.6.0a0 Schrödinger, LLC).

Growth Tests. Growth tests of yeast strains on YP agar plates were conducted as described previously.[15] The strains were grown in SD medium, without tryptophan as necessary. Tenfold serial dilutions of SD cultures with OD_{600} = 1, 0.1, 0.01, and 0.001 were then spotted on YPD and YPA agar plates. The plates were incubated for 3 days at 30 °C.

Western Blotting of Flag-Tag. Mitochondrial fractions were prepared from yeast strains grown in CMLE. 10 μg protein samples were separated by 10% Laemmli SDS-PAGE and transferred to a PVDF membrane in the glycine-methanol transfer system. After probing the PVDF membrane with a primary anti-Flag antibody from rabbit (0.1 μg/mL; Sigma-Aldrich), the membrane was incubated with an anti-rabbit IgG secondary antibody conjugated with alkaline phosphatase (Promega).

Protein Concentrations. Protein concentrations were determined by the BCA method using BSA solutions as standards.

■ ASSOCIATED CONTENT

Supporting Information

The Supporting Information is available free of charge at https://pubs.acs.org/doi/10.1021/acsomega.4c02614.

> Comparison of protein sequences of bacterial and apicomplexan MQO; activity of mutated MQO; growth phenotypes of yeast strains; superimposition of FAD-binding sites; PCR primers used in this study (PDF)

■ AUTHOR INFORMATION

Corresponding Author

Takeshi Ito − *Institute of Advanced Medical Sciences, Tokushima University, Tokushima 770-8503, Japan; Graduate School of Pharmaceutical Sciences, Tokushima University, Tokushima 770-8503, Japan;* Present Address: Graduate School of Agriculture, Ehime University. The author also conducted considerable work at the current address; orcid.org/0000-0001-7739-8705; Email: ito.takeshi.rp@ehime-u.ac.jp

Authors

Yuma Tojo − *Institute of Advanced Medical Sciences, Tokushima University, Tokushima 770-8503, Japan; Faculty of Pharmaceutical Sciences, Tokushima University, Tokushima 770-8503, Japan*

Minori Fujii − *Institute of Advanced Medical Sciences, Tokushima University, Tokushima 770-8503, Japan; Faculty of Pharmaceutical Sciences, Tokushima University, Tokushima 770-8503, Japan*

https://doi.org/10.1021/acsomega.4c02614
ACS Omega 2024, 9, 21647−21657

Kohei Nishino − *Institute of Advanced Medical Sciences, Tokushima University, Tokushima 770-8503, Japan*
Hidetaka Kosako − *Institute of Advanced Medical Sciences, Tokushima University, Tokushima 770-8503, Japan;* orcid.org/0000-0003-3228-6368
Yasuo Shinohara − *Institute of Advanced Medical Sciences, Tokushima University, Tokushima 770-8503, Japan; Graduate School of Pharmaceutical Sciences, Tokushima University, Tokushima 770-8503, Japan*

Complete contact information is available at: https://pubs.acs.org/10.1021/acsomega.4c02614

Author Contributions

#Y.T. and M.F. contributed equally

Notes

The authors declare no competing financial interest.

■ ACKNOWLEDGMENTS

This work was supported by JSPS KAKENHI Grant Number JP22K14838, the research program for the development of intelligent Tokushima artificial exosome (iTEX) from Tokushima University, and the Joint Usage and Joint Research Programs, the Institute of Advanced Medical Sciences, Tokushima University. We thank the equipment support provided by the Institute of Advanced Medical Sciences, Tokushima University.

■ REFERENCES

(1) Gardner, M. J.; Hall, N.; Fung, E.; White, O.; Berriman, M.; Hyman, R. W.; Carlton, J. M.; Pain, A.; Nelson, K. E.; Bowman, S.; et al. Genome sequence of the human malaria parasite Plasmodium falciparum. *Nature* **2002**, *419*, 498−511.
(2) Nosenko, T.; Bhattacharya, D. Horizontal gene transfer in chromalveolates. *BMC Evol. Biol.* **2007**, *7*, 173.
(3) Hayward, J. A.; van Dooren, G. G. Same same, but different: Uncovering unique features of the mitochondrial respiratory chain of apicomplexans. *Mol. Biochem. Parasitol.* **2019**, *232*, 111204.
(4) Maclean, A. E.; Hayward, J. A.; Huet, D.; van Dooren, G. G.; Sheiner, L. The mystery of massive mitochondrial complexes: The apicomplexan respiratory chain. *Trends Parasitol.* **2022**, *38*, 1041−1052.
(5) Lang-Unnasch, N. Purification and properties of Plasmodium falciparum malate dehydrogenase. *Mol. Biochem. Parasitol.* **1992**, *50*, 17−25.
(6) Chan, M.; Sim, T. S. Functional characterization of an alternative [lactate dehydrogenase-like] malate dehydrogenase in Plasmodium falciparum. *Parasitol. Res.* **2004**, *92*, 43−47.
(7) Tripathi, A. K.; Desai, P. V.; Pradhan, A.; Khan, S. I.; Avery, M. A.; Walker, L. A.; Tekwani, B. L. An alpha-proteobacterial type malate dehydrogenase may complement LDH function in Plasmodium falciparum. Cloning and biochemical characterization of the enzyme. *Eur. J. Biochem.* **2004**, *271*, 3488−3502.
(8) Ke, H.; Lewis, I. A.; Morrisey, J. M.; McLean, K. J.; Ganesan, S. M.; Painter, H. J.; Mather, M. W.; Jacobs-Lorena, M.; Llinás, M.; Vaidya, A. B. Genetic investigation of tricarboxylic acid metabolism during the Plasmodium falciparum life cycle. *Cell Rep.* **2015**, *11*, 164−174.
(9) Uyemura, S. A.; Luo, S.; Vieira, M.; Moreno, S. N.; Docampo, R. Oxidative phosphorylation and rotenone-insensitive malate- and NADH-quinone oxidoreductases in Plasmodium yoelii yoelii mitochondria in situ. *J. Biol. Chem.* **2004**, *279*, 385−393.
(10) Mogi, T.; Kita, K. Diversity in mitochondrial metabolic pathways in parasitic protists Plasmodium and Cryptosporidium. *Parasitol. Int.* **2010**, *59*, 305−312.
(11) Jacot, D.; Waller, R. F.; Soldati-Favre, D.; MacPherson, D. A.; MacRae, J. I. Apicomplexan Energy Metabolism: Carbon Source Promiscuity and the Quiescence Hyperbole. *Trends. Parasitol.* **2016**, *32*, 56−70.
(12) Hartuti, E. D.; Inaoka, D. K.; Komatsuya, K.; Miyazaki, Y.; Miller, R. J.; Xinying, W.; Sadikin, M.; Prabandari, E. E.; Waluyo, D.; Kuroda, M.; et al. Biochemical studies of membrane bound Plasmodium falciparum mitochondrial L-malate: Quinone oxidoreductase, a potential drug target. *Biochim. Biophys. Acta, Bioenerg.* **2018**, *1859*, 191−200.
(13) Lunev, S.; Batista, F. A.; Bosch, S. S.; Wrenger, C.; Groves, M. R. *Identification and Validation of Novel Drug Targets for the Treatment of Plasmodium falciparum Malaria: New Insights*; IntechOpen, 2016. DOI: 10.5772/65659.
(14) Wang, X.; Miyazaki, Y.; Inaoka, D. K.; Hartuti, E. D.; Watanabe, Y. I.; Shiba, T.; Harada, S.; Saimoto, H.; Burrows, J. N.; Benito, F. J. G.; et al. Identification of Plasmodium falciparum Mitochondrial Malate: Quinone Oxidoreductase Inhibitors from the Pathogen Box. *Genes* **2019**, *10* (6), 471.
(15) Ito, T.; Kajita, S.; Fujii, M.; Shinohara, Y. Plasmodium Parasite Malate-Quinone Oxidoreductase Functionally Complements a Yeast Deletion Mutant of Mitochondrial Malate Dehydrogenase. *Microbiol. Spectr* **2023**, *11* (3), No. e0016823.
(16) Acharjee, R.; Talaam, K. K.; Hartuti, E. D.; Matsuo, Y.; Sakura, T.; Gloria, B. M.; Hidano, S.; Kido, Y.; Mori, M.; Shiomi, K.; et al. Biochemical Studies of Mitochondrial Malate: Quinone Oxidoreductase from Toxoplasma gondii. *Int. J. Mol. Sci.* **2021**, *22*, 7830.
(17) Kabongo, A. T.; Acharjee, R.; Sakura, T.; Bundutidi, G. M.; Hartuti, E. D.; Davies, C.; Gundogdu, O.; Kita, K.; Shiba, T.; Inaoka, D. K. Biochemical characterization and identification of ferulenol and embelin as potent inhibitors of malate: Quinone oxidoreductase from Campylobacter jejuni. *Front. Mol. Biosci.* **2023**, *10*, 1095026.
(18) Varadi, M.; Velankar, S. The impact of AlphaFold Protein Structure Database on the fields of life sciences. *Proteomics* **2023**, *23*, 2200128.
(19) Jumper, J.; Evans, R.; Pritzel, A.; Green, T.; Figurnov, M.; Ronneberger, O.; Tunyasuvunakool, K.; Bates, R.; Žídek, A.; Potapenko, A.; et al. Highly accurate protein structure prediction with AlphaFold. *Nature* **2021**, *596*, 583−589.
(20) Baek, M.; DiMaio, F.; Anishchenko, I.; Dauparas, J.; Ovchinnikov, S.; Lee, G. R.; Wang, J.; Cong, Q.; Kinch, L. N.; Schaeffer, R. D.; et al. Accurate prediction of protein structures and interactions using a three-track neural network. *Science* **2021**, *373*, 871−876.
(21) Varadi, M.; Anyango, S.; Deshpande, M.; Nair, S.; Natassia, C.; Yordanova, G.; Yuan, D.; Stroe, O.; Wood, G.; Laydon, A.; et al. AlphaFold Protein Structure Database: Massively expanding the structural coverage of protein-sequence space with high-accuracy models. *Nucleic Acids Res.* **2022**, *50*, D439−D444.
(22) Hekkelman, M. L.; de Vries, I.; Joosten, R. P.; Perrakis, A. AlphaFill: Enriching AlphaFold models with ligands and cofactors. *Nat. Methods* **2023**, *20*, 205−213.
(23) Subramaniam, S.; Kleywegt, G. J. A paradigm shift in structural biology. *Nat. Methods* **2022**, *19*, 20−23.
(24) Suckau, D.; Mak, M.; Przybylski, M. Protein surface topology-probing by selective chemical modification and mass spectrometric peptide mapping. *Proc. Natl. Acad. Sci. U. S. A.* **1992**, *89*, 5630−5634.
(25) Glocker, M. O.; Borchers, C.; Fiedler, W.; Suckau, D.; Przybylski, M. Molecular characterization of surface topology in protein tertiary structures by amino-acylation and mass spectrometric peptide mapping. *Bioconjugate Chem.* **1994**, *5*, 583−590.
(26) Liu, X. R.; Zhang, M. M.; Gross, M. L. Mass Spectrometry-Based Protein Footprinting for Higher-Order Structure Analysis: Fundamentals and Applications. *Chem. Rev.* **2020**, *120*, 4355−4454.
(27) Fraenkel-Conrat, H. Methods for investigating the essential groups for enzyme activity. *Methods Enzymol.* **1957**, *4*, 247−269.
(28) Petrotchenko, E. V.; Borchers, C. H. Protein Chemistry Combined with Mass Spectrometry for Protein Structure Determination. *Chem. Rev.* **2022**, *122*, 7488−7499.

(29) Kanda, Y. Investigation of the freely available easy-to-use software'EZR' for medical statistics. *Bone Marrow Transplant.* **2013**, *48*, 452−458.
(30) Ghanta, S.; Grossmann, R. E.; Brenner, C. Mitochondrial protein acetylation as a cell-intrinsic, evolutionary driver of fat storage: Chemical and metabolic logic of acetyl-lysine modifications. *Crit. Rev. Biochem. Mol. Biol.* **2013**, *48*, 561−574.
(31) Taus, T.; Köcher, T.; Pichler, P.; Paschke, C.; Schmidt, A.; Henrich, C.; Mechtler, K. Universal and confident phosphorylation site localization using phosphoRS. *J. Proteome Res.* **2011**, *10*, 5354−5362.
(32) Fukasawa, Y.; Tsuji, J.; Fu, S. C.; Tomii, K.; Horton, P.; Imai, K. MitoFates: Improved prediction of mitochondrial targeting sequences and their cleavage sites. *Mol. Cell. Proteomics* **2015**, *14*, 1113−1126.
(33) Birktoft, J. J.; Banaszak, L. J. The presence of a histidine-aspartic acid pair in the active site of 2-hydroxyacid dehydrogenases. X-ray refinement of cytoplasmic malate dehydrogenase. *J. Biol. Chem.* **1983**, *258*, 472−482.
(34) Holliday, G. L.; Mitchell, J. B.; Thornton, J. M. Understanding the functional roles of amino acid residues in enzyme catalysis. *J. Mol. Biol.* **2009**, *390*, 560−577.
(35) Ho, S. N.; Hunt, H. D.; Horton, R. M.; Pullen, J. K.; Pease, L. R. Site-directed mutagenesis by overlap extension using the polymerase chain reaction. *Gene* **1989**, *77*, 51−59.
(36) Belikova, Y. O.; Kotlyar, A. B.; Vinogradov, A. D. Oxidation of malate by the mitochondrial succinate-ubiquinone reductase. *Biochim. Biophys. Acta* **1988**, *936*, 1−9.
(37) Niehaus, T. D.; Hillmann, K. B. Enzyme promiscuity, metabolite damage, and metabolite damage control systems of the tricarboxylic acid cycle. *Febs J.* **2020**, *287*, 1343−1358.
(38) Schneider, C. A.; Rasband, W. S.; Eliceiri, K. W. NIH Image to ImageJ: 25 years of image analysis. *Nat. Methods* **2012**, *9*, 671−675.
(39) Ohgane, K.; Yoshioka, H. *Quantification of Gel Bands by an Image J. Macro, Band/Peak Quantification Tool*, 2019. DOI: 10.17504/protocols.io.7vghn3w
(40) Iwasaki, W.; Tachiwana, H.; Kawaguchi, K.; Shibata, T.; Kagawa, W.; Kurumizaka, H. Comprehensive structural analysis of mutant nucleosomes containing lysine to glutamine (KQ) substitutions in the H3 and H4 histone-fold domains. *Biochemistry* **2011**, *50*, 7822−7832.
(41) Elkhal, C. K.; Kean, K. M.; Parsonage, D.; Maenpuen, S.; Chaiyen, P.; Claiborne, A.; Karplus, P. A. Structure and proposed mechanism of L-α-glycerophosphate oxidase from Mycoplasma pneumoniae. *Febs J.* **2015**, *282*, 3030−3042.
(42) Yang, J.; Chen, X.; Jin, S.; Ding, J. Structure and biochemical characterization of l-2-hydroxyglutarate dehydrogenase and its role in the pathogenesis of l-2-hydroxyglutaric aciduria. *J. Biol. Chem.* **2024**, *300*, 105491.
(43) Minárik, P.; Tomásková, N.; Kollárová, M.; Antalík, M. Malate dehydrogenases–structure and function. *Gen. Physiol. Biophys.* **2002**, *21* (3), 257−265.
(44) Mogi, T.; Murase, Y.; Mori, M.; Shiomi, K.; Omura, S.; Paranagama, M. P.; Kita, K. Polymyxin B identified as an inhibitor of alternative NADH dehydrogenase and malate: Quinone oxidoreductase from the Gram-positive bacterium Mycobacterium smegmatis. *J. Biochem.* **2009**, *146*, 491−499.
(45) Spahich, N. A.; Vitko, N. P.; Thurlow, L. R.; Temple, B.; Richardson, A. R. Staphylococcus aureus lactate- and malate-quinone oxidoreductases contribute to nitric oxide resistance and virulence. *Mol. Microbiol.* **2016**, *100*, 759−773.
(46) Okun, J. G.; Lümmen, P.; Brandt, U. Three classes of inhibitors share a common binding domain in mitochondrial complex I (NADH: Ubiquinone oxidoreductase). *J. Biol. Chem.* **1999**, *274*, 2625−2630.
(47) Yu, C. A.; Xia, D.; Kim, H.; Deisenhofer, J.; Zhang, L.; Kachurin, A. M.; Yu, L. Structural basis of functions of the mitochondrial cytochrome bc1 complex. *Biochim. Biophys. Acta* **1998**, *1365*, 151−158.
(48) Miyadera, H.; Shiomi, K.; Ui, H.; Yamaguchi, Y.; Masuma, R.; Tomoda, H.; Miyoshi, H.; Osanai, A.; Kita, K.; Omura, S. Atpenins, potent and specific inhibitors of mitochondrial complex II (succinate-ubiquinone oxidoreductase). *Proc. Natl. Acad. Sci. U. S. A.* **2003**, *100*, 473−477.
(49) Hidayati, A. R.; MelindaIlmi, M.; Ilmi, H.; Sakura, T.; Sakaguchi, M.; Ohmori, J.; Hartuti, E. D.; Tumewu, L.; Inaoka, D. K.; Tanjung, M.; et al. Effect of geranylated dihydrochalcone from Artocarpus altilis leaves extract on Plasmodium falciparum ultra-structural changes and mitochondrial malate: Quinone oxidoreductase. *Int. J. Parasitol.: Drugs Drug Resist.* **2023**, *21*, 40−50.
(50) Cahyono, A. W.; Fitri, L. E.; Winarsih, S.; Prabandari, E. E.; Waluyo, D.; Pramisandi, A.; Chrisnayanti, E.; Dewi, D.; Siska, E.; Nurlaila, N.; et al. Nornidulin, A New Inhibitor of Plasmodium falciparum Malate: Quinone Oxidoreductase (PfMQO) from Indonesian Aspergillus sp. BioMCC f.T.8501. *Pharmaceuticals* **2023**, *16*, 268.
(51) Fernandes, J.; Weddle, A.; Kinter, C. S.; Humphries, K. M.; Mather, T.; Szweda, L. I.; Kinter, M. Lysine Acetylation Activates Mitochondrial Aconitase in the Heart. *Biochemistry* **2015**, *54*, 4008−4018.
(52) Zhao, S.; Xu, W.; Jiang, W.; Yu, W.; Lin, Y.; Zhang, T.; Yao, J.; Zhou, L.; Zeng, Y.; Li, H.; et al. Regulation of cellular metabolism by protein lysine acetylation. *Science* **2010**, *327*, 1000−1004.
(53) Kim, E. Y.; Kim, W. K.; Kang, H. J.; Kim, J. H.; Chung, S. J.; Seo, Y. S.; Park, S. G.; Lee, S. C.; Bae, K. H. Acetylation of malate dehydrogenase 1 promotes adipogenic differentiation via activating its enzymatic activity. *J. Lipid Res.* **2012**, *53*, 1864−1876.
(54) Hashimoto, M.; Shinohara, Y.; Majima, E.; Hatanaka, T.; Yamazaki, N.; Terada, H. Expression of the bovine heart mitochondrial ADP/ATP carrier in yeast mitochondria: Significantly enhanced expression by replacement of the N-terminal region of the bovine carrier by the corresponding regions of the yeast carriers. *Biochim. Biophys. Acta* **1999**, *1409*, 113−124.
(55) Kawai, S.; Hashimoto, W.; Murata, K. Transformation of Saccharomyces cerevisiae and other fungi: Methods and possible underlying mechanism. *Bioeng. Bugs* **2010**, *1*, 395−403.
(56) Mirdita, M.; Schütze, K.; Moriwaki, Y.; Heo, L.; Ovchinnikov, S.; Steinegger, M. ColabFold: Making protein folding accessible to all. *Nat. Methods* **2022**, *19*, 679−682.
(57) *ColabFold v1.5.3: AlphaFold2 using MMseqs2*. https://colab.research.google.com/github/sokrypton/ColabFold/blob/56c72044c7d51a311ca99b953a71e552fdc042e1/AlphaFold2.ipynb#scrollTo=G4yBrceuFbf3, (accessed 2023−December−21).

https://doi.org/10.1021/acsomega.4c02614
ACS Omega 2024, 9, 21647−21657